THE AMERICAN SOCIETY OF MECHANICAL ENGINEERS
345 E. 47th St., New York, N.Y. 10017

97-GT-399

BREAK

MODELING UNSTEADY BOUNDARY LAYER TRANSITION ON A CURVED PLATE UNDER PERIODIC UNSTEADY FLOW CONDITIONS: AERODYNAMIC AND HEAT TRANSFER INVESTIGATIONS

P. Chakka, M. T. Schobeiri
Turbomachinery Performance Laboratory
Texas A&M University
College Station, Texas

ABSTRACT

A boundary layer transition model is developed that accounts for the effects of periodic unsteady wake flow on the boundary layer transition. To establish the model, comprehensive unsteady boundary layer and heat transfer experimental investigations are conducted. The experiments are performed on a curved plate at zero-streamwise pressure gradient under periodic unsteady wake flow, where the frequency of the periodic unsteady flow is varied. The analysis of the time dependent velocities, turbulence intensities, and turbulence intermittencies has identified three distinct quantities as primarily responsible for the transition of an unsteady boundary layer. These quantities, which exhibit the basis of the transition model presented in this paper, are: (1) relative intermittency, (2) maximum intermittency, and (3) minimum intermittency. To validate the developed transition model, it is implemented in an existing boundary layer code, and the resulting velocity profiles and the heat transfer coefficients are compared with the experimental data.

NOMENCLATURE

b	=	intermittency wake width
C	=	threshold level
h	=	heat transfer coefficient (W/m^2K)
I(t)	=	step function(square wave)
Nu	=	Nusselt number based on concave arc length, $Nu = hs_0/k$
Pr	=	Prandtl number, $Pr = \nu/\alpha$
Re_x	=	local Reynolds number based on longitudinal distance, $Re_x = (\bar{U}\, s)/\nu$
$Re_{x,s}$	=	Reynolds number at the beginning of transition
$Re_{x,e}$	=	Reynolds number at the end of transition
s	=	longitudinal distance from plate leading edge (mm)
s_0	=	arc length of concave surface of curved plate, $s_0 = 690$ mm
s_R	=	rod spacing
S(t)	=	detector function
St	=	Stanton number, $St = h/(\rho C_p \bar{U})$
t	=	time (s)
T	=	time for one revolution of wake generator
Tu	=	reference turbulence intensity
<Tu>	=	ensemble-averaged reference turbulence intensity
U	=	instantaneous velocity (m/s)
$\bar{U}$	=	time-averaged velocity (m/s)
U_{in}	=	inlet velocity in streamwise direction (m/s)
U_w	=	circumferential velocity of the wake generator (m/s)
y	=	lateral distance from plate surface (mm)
α	=	thermal diffusivity (m^2/s)
$\langle\gamma(t)\rangle_{max}$	=	maximum ensemble-averaged intermittency
$\langle\gamma(t)\rangle_{min}$	=	minimum ensemble-averaged intermittency
$\bar{\gamma}$	=	time-averaged intermittency
$\langle\gamma(t)\rangle$	=	ensemble averaged intermittency
Γ	=	relative turbulence intermittency
ϵ_H	=	eddy diffusivity for heat
ζ	=	nondimensional coordinate, ξ_z/b
ν	=	kinematic viscosity of air (m^2/s)

Presented at the International Gas Turbine & Aeroengine Congress & Exhibition
Orlando, Florida — June 2–June 5, 1997
This paper has been accepted for publication in the Transactions of the ASME
Discussion of it will be accepted at ASME Headquarters until September 30, 1997

ξ_2 = transformed co-ordinate, $\xi_2 = t\, s_R/\tau$
ρ = density of air (kg/m^3)
σ = length spacing ratio, s_0/S_R
τ = one wake passing period
ϕ = velocity ratio, U_{in}/U_w
Ω = non-dimensionalized unsteady parameter, $\Omega = \sigma/\phi$

1. Introduction

The flow in a turbomachine stage is highly turbulent and unsteady due to the interactions between the stator and the rotor. The trailing edge thickness, together with the boundary layer thickness, in association with the rotational motion of the rotor generate unsteady wakes. The unsteady wake exhibits mean velocity defects with a high level of turbulence intensity that passes through the blade rows affecting the natural boundary layer transition. The effect of these wakes on boundary layer transition is important to the design of turbomachinery blades. Successful prediction of transition start and length would help in efficient design of turbine or compressor stages. However, the transition process under the influence of periodic unsteady wakes is not predicted reliably with the existing steady transition models. For this reason, the current investigation focuses on the transition process and its effect on the boundary layer velocity profiles and heat transfer coefficients under unsteady wake flow condition.

The transition process was first explained by Emmons(1950) through the turbulent spot production theory. This theory was later promoted by Dhawan and Narasimha(1958), who proposed a universal profile for intermittency factor for natural transition. Studies by Abu-Ghannam and Shaw(1980), Gostelow and Blunden(1989), Gostelow et al.(1995), Dullenkopf and Mayle(1994) were conducted to determine the effect of free-stream turbulence and pressure gradient on the spot production rate and the intermittency factor. Experiments for the effect of unsteady wake flow on the boundary layer transition were conducted by Walker(1989), Hodson(1990), Paxson and Mayle(1991) and Orth(1992). Hodson developed a method for calculating boundary layer parameters under unsteady flow conditions using the strip calculation method and the space-time diagrams. He compared the loss coefficient for a turbine blade calculated using the strip calculation method with the time-averaged results. Paxson and Mayle investigated the effect of unsteady passing wakes on the laminar boundary layer near the stagnation region. Dullenkopf and Mayle(1994) proposed a time averaged transition model. Although this model produces satisfactory results, it is not appropriate for the unsteady flow situation. Few of these researchers have addressed the effect of wake frequency and the structure on boundary layer transition.

The calculation of intermittency factor under the unsteady flow situation is a difficult task because of the free-stream, which periodically changes from almost non-turbulent to high turbulent intensity values. The process of turbulent/non-turbulent decisions from the instantaneous signals measured under these unsteady conditions is reviewed by Hedley and Keffer(1974). They proposed derivatives of velocity signals as the detector function to identify the turbulent and non-turbulent parts in the signals. This method was also used by Antonia and Bradshaw(1971), Kovasznay et al.(1970), and Bradshaw and Murlis(1973). Mayle and Paxson(1991) and Mayle(1991) used a similar method for unsteady flows.

Significant contributions to unsteady boundary layer research were made by Pfeil and his co-researchers(Pache 1976, Eifler 1975, Schobeiri 1979, Herbst 1980, Orth 1991). Pfeil and Herbst(1979), using the squirrel cage type wake generator and a flat plate, developed a wake-induced transition model that is now generally accepted as correct. They also showed that in between the induced transition regions by wakes, the boundary layer grew naturally. Comprehensive investigations on the effect of periodic unsteady flow on a curved plate were performed by Schobeiri and Radke(1994b), and Schobeiri et al.(1995). They showed that an increase in wake passing frequency as a result of reducing the wake spacing results in changing the wake turbulence structure and a shift of transition region towards the leading edge.

Development of an accurate unsteady transition model is essential in predicting the unsteady boundary layer characteristics such as skin friction and heat transfer coefficients. With an appropriate transition model, it is possible to solve the boundary layer equations numerically using the methods proposed by Launder and Spalding(1972), Crawford and Kays(1976), and Schmidt and Patankar(1991). Bearing this in mind, the current investigation focuses on the calculation of the intermittency factor and development of an unsteady model that can be used in Navier-Stokes and boundary layer codes to predict the parameters necessary for the efficient design of turbomachinery stages.

The present investigation includes aerodynamic and heat transfer experiments detailed in section 2 to provide a comprehensive set of data. Instantaneous velocity signals are used to determine the intermittency throughout the boundary layer. Details on the calculation and analysis of intermittency for unsteady flows is discussed in section 3. The implementation of the model in the boundary layer code is explained in section 4, followed by the results and discussion.

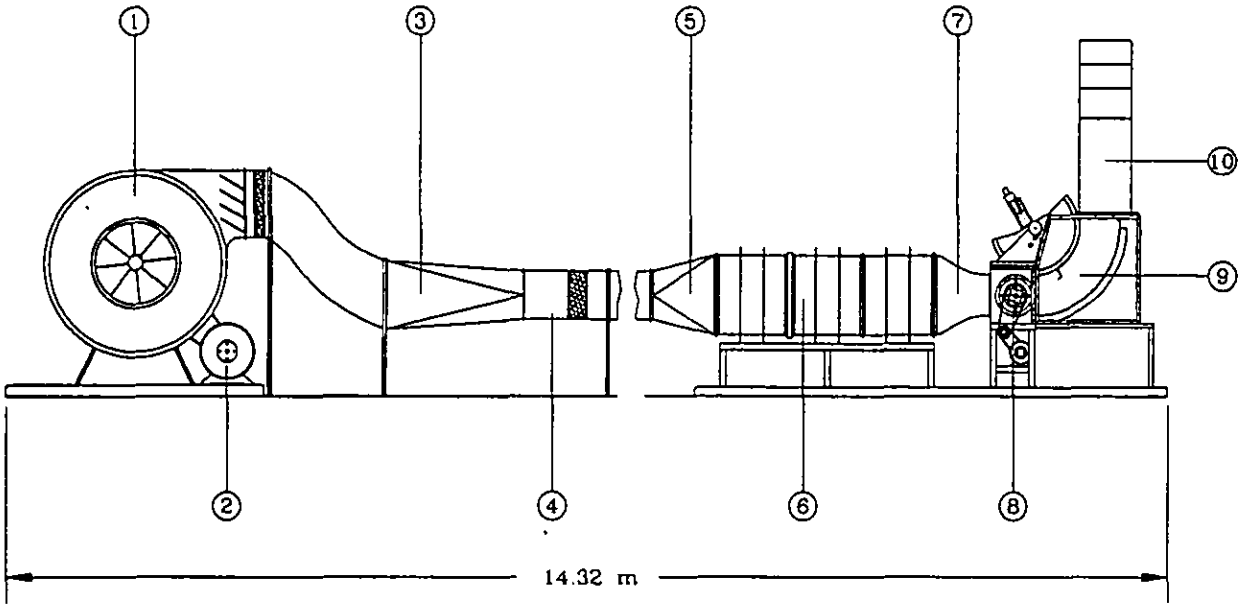

Figure 1. Overall layout of the test facility: 1. Fan, 2. Motor, 3. Transition duct, 4. Straight pipe, 5. Diffuser, 6. Settling Chamber, 7. Nozzle, 8. Wake generator, 9. Test section, 10. Exit duct.

Table 1: Specifications of inlet flow and wake generator characteristics

Parameters	Values	Parameters	Values
Nozzle exit Reynolds number	$Re_h = 0.43 \times 10^6$	Nozzle exit turbulence intensity	Tu = 1.20%
Nozzle exit height	h = 420.00 mm	Nozzle exit width	w = 593.00mm
Rod diameter	d_R = 2 mm	Radius of curvature of curved plate	r = 702.5 mm
Steady reference (no rods)	$s_R = \infty$ mm	Ω - parameter steady case	Ω = 0.0
Set 1 rod spacing	s_R = 314.0 mm	Ω - parameter for set 1	Ω = 1.033
Set 2 rod spacing	s_R = 188.4 mm	Ω - parameter for set 2	Ω = 1.725
Set 3 rod spacing	s_R = 94.2 mm	Ω - parameter for set 3	Ω = 3.443
Set 4 rod spacing	s_R = 62.8 mm	Ω - parameter for set 4	Ω = 5.166
No. of rods in set 1	n_R = 3	No. of rods in set 2	n_R = 5
No. of rods in set 3	n_R = 10	No. of rods in set 4	n_R = 15

2. EXPERIMENTAL INVESTIGATIONS

To understand the effect of wakes on the aerodynamic and heat transfer characteristics, detailed experiments are performed on the curved plates. The experimental data are collected using a subsonic wind tunnel test facility, which is shown in Fig. 1. Since this facility was already described by Schobeiri and Radke (1994) and Schobeiri et al. (1995) only a brief description will be given below.

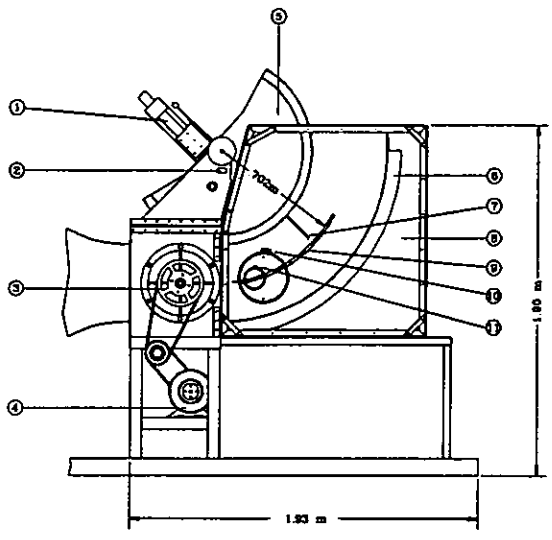

Figure 2. Test Section: 1. Traversing system, 2. Nozzle, 3. Wake generator, 4. Electric motor, 5. Convex wall, 6. Concave wall, 7. Hot-wire probe, 8. Plexiglass wall, 9. Curved plate, 10. Small vernier, 11. Large Vernier.

The facility consists of a large centrifugal fan, a settling chamber, a nozzle, a wake generator, and a curved test section. Through the use of a throttle mechanism located at the exit of the fan, the velocity at the inlet of the test section is set at 11 m/s. The rest of the inlet flow conditions can be found in Table 1. The free-stream turbulence intensity of steady flow into the test section is about 1.2 %. As explained by Schobeiri and Radke(1994), the facility was designed to generate a turbulence intensity about 1% without wakes. For unsteady flow cases, however, higher free stream turbulence intensities are established by secondary wakes.

The *squirrel cage* type wake generator shown in Fig. 2 is used to generate the unsteady flow condition present at the inlet of the test section. The wake generator consists of two parallel rotating, circular disks in which rods can be arranged circumferentially. To determine the effect of wake passing frequency and structure on boundary layer transition, five different rod spacings are used(see Table 1). The unsteady flow produced by the wake generator is characterized by an unsteady parameter Ω. This parameter is similar to the Strouhal number and is defined as $\Omega = \sigma/\phi$ where σ is the ratio of the arc length of the plate s_o and the spacing between the rods s_R, and ϕ is the ratio of the inlet velocity U_{in} and the circumferential velocity of the wake generator U_w. Physically, Ω is the ratio of the transit time of the flow across the test section to the wake passing period. The values of Ω cover a broad range that are typical of a turbomachine and they are specified in Table 1.

Two distinct curved plates, which simulate the pressure surface of a turbine blade, were utilized in this investigation. The first was a curved plate for aerodynamic measurements and the second a heat transfer curved plate with the same concave dimensions as the aerodynamic plate. The test section with the wake generator, curved plate, and the instrumentation is shown in Fig. 2. Boundary layer measurements were taken on the aerodynamic curved plate and heat transfer plate(heater foil not energized) and temperature measurements were taken on the heat transfer plate with liquid crystal instrumentation. All measurements were taken on the concave surface of the curved plate only. For a detailed discussion of boundary layer measurements, we refer to Schobeiri and Radke(1994) and Schobeiri et al.(1995). The heat transfer measurements are discussed in detail by Wright and Schobeiri(1996). Boundary layer measurements were taken on the concave surface of the aerodynamic plate for Ω= 0, 1.033, 1.725, 3.443, and 5.116 using a TSI single-wire hot-wire probe with a 4µm tungsten filament. The probe was mounted on a computer controlled linear traversing system. This system is capable of traversing in increments of 2.5 µm, which is essential in measuring the

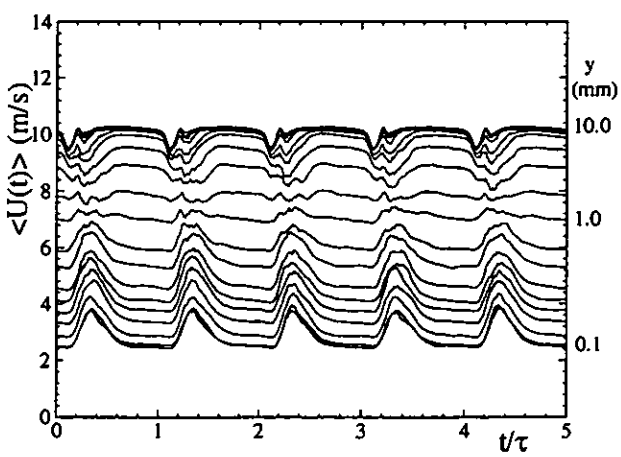

Figure 3. Ensemble-averaged velocity distribution as a function of non-dimensional time at different y-locations at $s/s_0 = 0.25$ for $\Omega = 1.725$(5-rods).

laminar-sublayer. To capture the major portion of the transition onset, the probe was traversed in the longitudinal direction in steps of 2° until 50 percent of the plate was reached. The next 25 percent of the plate was traversed in increments of 3°, and the last quarter was traversed in increments of 5°. For each streamwise position, the boundary layer measurements were started 0.1 mm above the surface of the plate and extended until 10.0 mm above the curved plate. Starting with a high sampling frequency of 10,240 Hz, the preliminary frequency variations showed that the same velocity, turbulence intensity, and intermittency can be reproduced with reduced sampling frequencies. Spectral analysis revealed that the sampling frequency of 2560 Hz is sufficient for boundary layer investigations. Thus, this frequency was chosen for all Ω values. Aerodynamic measurements were taken on the heat transfer plate to insure that the new plate provided similar boundary layer result so that a comparison could be made between the boundary layer measurements and the heat transfer measurements.

The power required for heating the heat transfer blade is supplied by a Sorensen DCR40-70B DC power supply. The current passing through the test blade is measured with a multimeter connected across a shunt resistor. A separate multimeter is connected across the output leads of the power supply to measure the voltage. The yellow band of the liquid is used for recording the data. The location of the yellow band is controlled through the power supply to the heater plate and the voltage and the current reading are recorded for different locations of the yellow band on the curved plate. The data are collected for the concave and the convex side of the curved plate. Note that no effect of Görtler vortices in the spanwise direction is observed while taking the liquid crystal measurements. We refer to Schobeiri and Radke(1994) for a discussion of the effect of curvature and Görtler vortices on boundary layer transition.

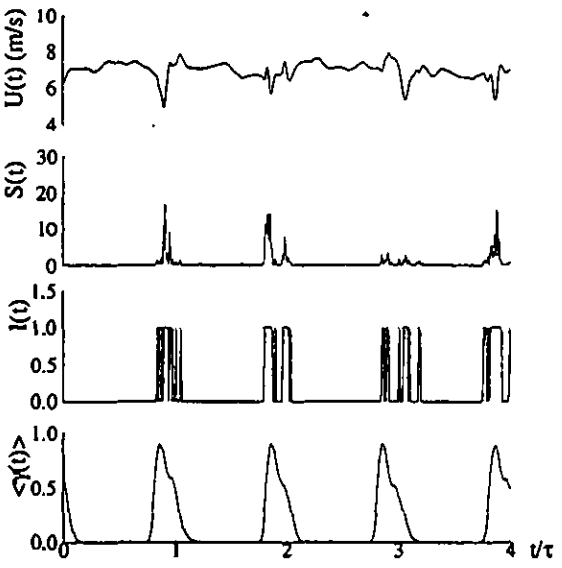

Figure 4. Calculation of ensemble averaged intermittency function from instantaneous velocities for Ω = 1.725(5-rods) and y = 0.1 mm.

3. INTERMITTENCY ANALYSIS

Intermittency distribution that identifies the flow being laminar or turbulent inside the boundary layer is calculated following the method of Hedley and Keffer (1974). Instantaneous velocities are used to identify this intermittency distribution. Representative plots of ensemble-averaged velocity signal are given in Fig. 3 inside the boundary layer. The instantaneous velocity is sensitized to increase its

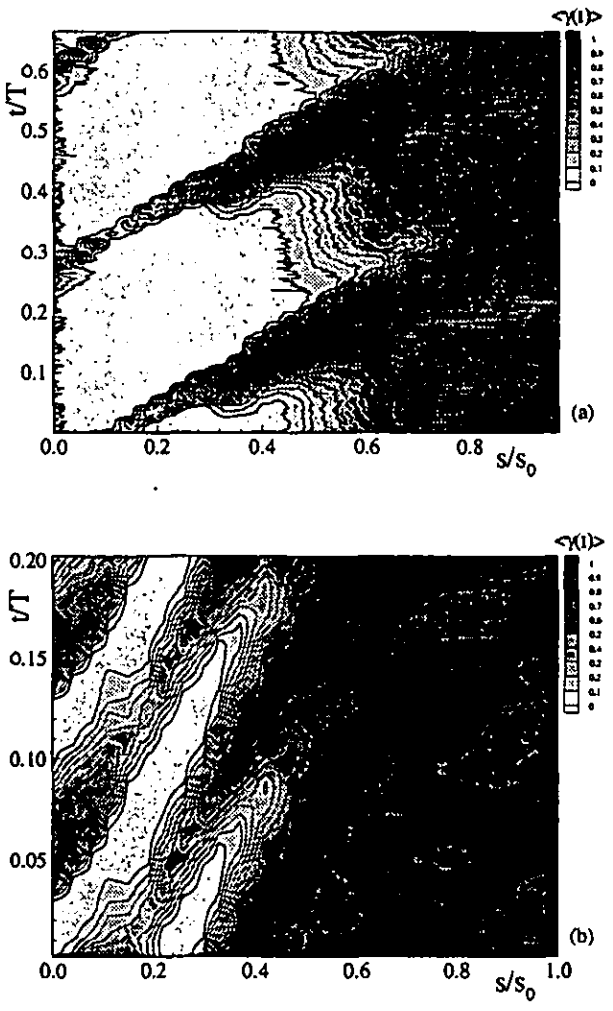

Figure 5(a and b). Contour plots of intermittency factor as a function of normalized axial distance s/s_0 for (a) Ω = 1.033 (3-rods) and (b) Ω = 3.443(10-rods) at y = 0.1 mm.

discriminatory capabilities between turbulent and non-turbulent parts of the signal. For this purpose, the second derivative of the velocity signal is used and squared for further analysis, and is called the detector function, S(t). Several other detector functions were used by Antonia and Bradshaw (1971), Antonia (1972), and Kowasznay et al. (1970). A threshold level C is then applied to this detector function to distinguish between the true turbulence and the signal *noise*.

$$I(t)=\begin{cases} 1 & when \quad S(t) \geq C, \\ 0 & when \quad S(t) < C. \end{cases} \qquad (1)$$

After applying the threshold level to the detector function S(t), the result is a random square wave with 0's representing the laminar case and 1's representing the turbulent behavior of the boundary layer. This square wave is ensemble averaged to get the ensemble averaged intermittency as follows

$$\langle \gamma_i(t_i) \rangle = \frac{1}{n}\sum_{j=1}^{n} I_{ij}(t_i) \qquad (2)$$

where n is the number of revolutions of the wake generator for which the data are collected. For time averaged intermittency, $\langle \gamma_i(t_i) \rangle$ is integrated with respect to time to give

$$\overline{\gamma}=\frac{1}{T}\int_{t=0}^{T} \langle \gamma_i(t_i) \rangle dt \qquad (3)$$

Figure 4 shows the processing of instantaneous velocities. Ensemble-averaged intermittency distribution as a function of non-dimensional time is shown in Figs. 5a and b for 3-rod and 10-rod cases. Similar plots are seen for other rod cases. Only the first two wakes are plotted for a better comparison of the effects of impinging wake frequency on the transition process. Intermittency is approximately equal to zero outside the wake region near the leading edge showing the non-turbulent behavior of the flow. The wake is represented by a thin strip with intermittency values near one, typical of a turbulent flow. As these wakes pass through the channel, the boundary layer periodically switches from laminar to turbulent depending on the presence of the wakes. The natural transition of the boundary layer is affected by periodic passing of wakes resulting in wake induced transition. The intermittency distributions in Figs. 5a and b show clearly the unsteady nature of the boundary layer transition. However, in this form, they cannot be used to quantitatively describe the complex unsteady transition process. To establish the basic relations essential for a quantitative description of the unsteady boundary layer transition, we resort to the fundamental studies

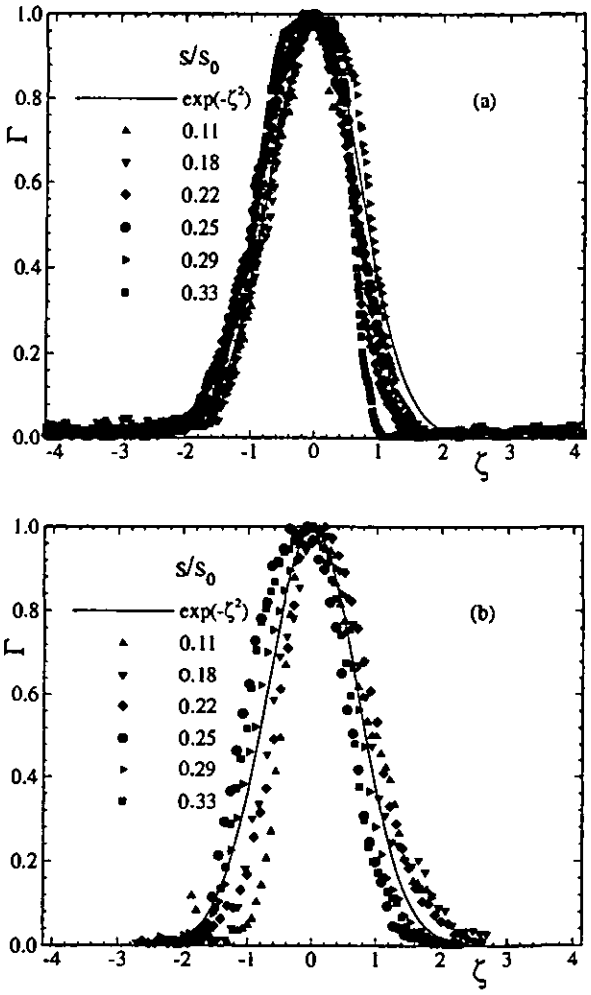

Figure 6(a and b). Relative intermittency as a function of non-dimensionalized lateral coordinate for (a) Ω = 1.033(3-rods) and (b) Ω = 3.443(10-rods) at y = 0.1 mm.

by Schobeiri and his co-workers (Schobeiri et. al (1996a), Schobeiri et. al (1996b), John and Schobeiri (1996) that deal with the physics of steady and unsteady wake development in a curved environment. These studies clearly show that the turbulence structure of the steady and unsteady wake flow is determined by the wake defect, which is a Gaussian function. Following the above studies, we define a dimensionless parameter :

$$\zeta = \frac{tU_w}{b} = \frac{ts_R}{\tau b} = \frac{\xi_2}{b} \text{ with } b = \frac{1}{\sqrt{\pi}}\int_{-\infty}^{+\infty} \Gamma \, d\xi_2 \qquad (4)$$

that relates the passing time t of a wake impinging on the plate surface with the wake passing velocity in the lateral direction U_w and the intermittency width b. The latter is directly related to the wake width introduced by Schobeiri and his co-workers.

In an analogous way to find the defect function, we define the relative intermittency Γ as:

$$\Gamma = \frac{\langle\gamma_i(t_i)\rangle - \langle\gamma_i(t_i)\rangle_{min}}{\langle\gamma_i(t_i)\rangle_{max} - \langle\gamma_i(t_i)\rangle_{min}} \qquad (5)$$

In the above equation, $\langle\gamma_i(t_i)\rangle$ is the time dependent ensemble-averaged intermittency function, which determines the transitional nature of an unsteady boundary layer. The maximum intermittency $\langle\gamma_i(t_i)\rangle_{max}$ exhibits the time dependent ensemble averaged intermittency value inside the wake vortical core. Finally, the minimum intermittency $\langle\gamma_i(t_i)\rangle_{min}$ represents the ensemble averaged intermittency values outside the wake vortical core. The relative intermittency function Γ is shown in Figs. 6a and b, for frequency values of Ω = 1.033(3-rods) and 3.443(10-rods) respectively with the dimensionless longitudinal distance s/s_o as a parameter. Again, similar results are observed for other rod frequencies listed in Table 1. The symbols represent the experimental data. For the reduced frequencies and longitudinal positions presented in these plots, the measured relative intermittency functions for wakes impinging on the plate surface follow very closely a Gaussian distribution, given by:

$$\Gamma = e^{-\zeta^2} \qquad (6)$$

Here, ζ is the non-dimensionalized lateral length scale. Using this function as a generally valid intermittency relationship for zero-pressure gradient cases, the intermittency function $\langle\gamma_i(t_i)\rangle$ is completely determined if additional information about the minimum and the maximum intermittency functions $\langle\gamma_i(t_i)\rangle_{min}$ and $\langle\gamma_i(t_i)\rangle_{max}$ are available. The distribution of $\langle\gamma_i(t_i)\rangle_{min}$ and $\langle\gamma_i(t_i)\rangle_{max}$ in streamwise direction are plotted in Fig. 8 for Ω = 1.033(3-rods). The steady case (no-rod case) shown in Fig. 7 serves as the basis of comparison for these maximum and minimum values. In the steady case, the intermittency starts to rise from zero at a streamwise Reynolds number $Re_{x,s} = 2x10^5$ and gradually equals unity corresponding to the fully turbulent state. This is typical of natural transition and follows the intermittency function introduced by Narasimha (1957). The distributions of maximum and minimum turbulence intermittencies $\langle\gamma_i(t_i)\rangle_{min}$ and $\langle\gamma_i(t_i)\rangle_{max}$ in the streamwise direction are shown in Fig. 8. For each particular streamwise location on the blade surface with a streamwise Reynolds number, for example $Re_{x,s} = 1x10^5$, two corresponding distinctively different intermittency states are periodically present. At this location, $\langle\gamma_i(t_i)\rangle_{max}$

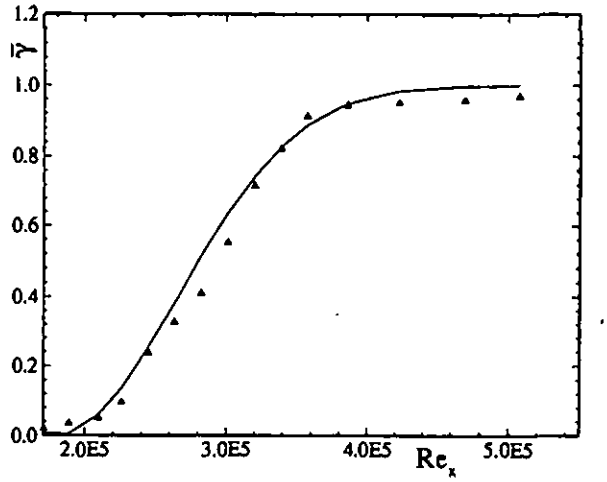

Figure 7. Intermittency as a function of Re_x for no-rod or steady case on the concave surface of the curved plate at y = 0.1 mm.

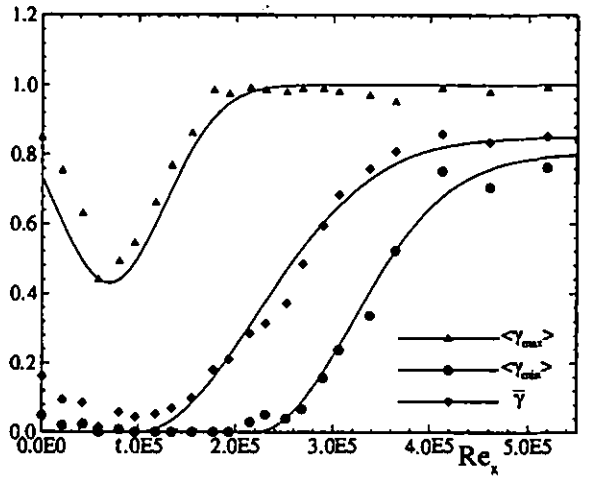

Figure 8. Maximum, minimum and time-averaged intermittency distributions as a function of axial Reynolds number for Ω = 1.033(3-rods) at y = 0.1 mm.

corresponds to the condition when the wake with its high turbulence intensity core impinges on the plate surface. Once the wake has passed over the surface, the same streamwise location is exposed to a low turbulence intensity flow regime with an intermittency state of $\langle\gamma_i(t_i)\rangle_{min}$, where no wake is present. As seen, $\langle\gamma_i(t_i)\rangle_{min}$ tends to follow the course of steady (no-wake) intermittency distribution exhibited in Fig. 6, with a gradual increase from an initial *non-turbulent* state with a value of zero approaching a final state of 0.8. The final state does not approach to the fully turbulent value of 1.0 due to the *calming* effect of the boundary layer. This tendency is expected as $\langle\gamma_i(t_i)\rangle_{min}$ is calculated outside the wake region where turbulence intensity is relatively small. On the other hand, $\langle\gamma_i(t_i)\rangle_{max}$ reveals a fundamentally different behavior

that needs to be discussed further. As Fig. 8 shows, the wake flow with an intermittency close to 1 impinges on the blade surface. By convecting downstream, its turbulent fluctuations undergo a strong damping by the wall shear stress forces. The process of damping continues until $<\gamma_i(t_i)>_{max}$ reaches a minimum. At this point the wall shear forces are not able to further suppress the turbulent fluctuations. As a consequence, the intermittency again increases to approach unity, showing the combined effect of *wake induced* and *natural transition* due to increased turbulence intensity level. Figure 8 also shows the average intermittency that is a result of the integral effect of periodic wakes with respect to time. The maximum intermittency is described by

$$<\gamma(t)>_{max} = 1.0 - c_1 e^{-\left(\frac{Re_x - Re_{x,s}}{Re_{x,s} - Re_{x,e}}\right)^2} \qquad (7)$$

where the constant c_1 is dependent on Ω. The minimum intermittency described by:

$$<\gamma(t)>_{min} = c_2\left(1.0 - e^{-\left(\frac{Re_x - Re_{x,s}}{Re_{x,s} - Re_{x,e}}\right)^2}\right) \qquad (8)$$

where the constant c_2 is again dependent on Ω. And the time averaged intermittency is described by:

$$\overline{\gamma} = c_4\left(1.0 - c_3 e^{-\left(\frac{Re - Re_{x,s}}{Re_{x,s} - Re_{x,e}}\right)^2}\right) \qquad (9)$$

The four constants for the frequencies under investigation are given in Table 2. Constant c_1 represents the extent of wall damping(the magnitude of trough in $<\gamma_i(t_i)>_{max}$), whereas constant c_2 is introduced as the asymptotic value of the minimum intermittency. It can be seen from Table 2 that constant c_2 shows an increase in trend as the wake frequency is increased. Constants c_3 and c_4 give the combined effect of c_1 and c_2 for $\overline{\gamma}$. It is also possible to derive c_3 and c_4 from Eqn. 3 by back-working $<\gamma_i(t_i)>$ through Eqn. 5. For natural transition, all the above constants approach unity. Also, the Reynolds numbers at the start and end of transition, $Re_{x,s}$ and $Re_{x,e}$, differ for different wake frequencies. The values of $Re_{x,s}$ and $Re_{x,e}$, for the Ω values under investigation are shown in Fig. 9. It will be seen from this figure that the transition starts earlier as the wake frequency Ω is increased. Also, the wake-induced transition length is higher when compared to the steady or no-wake transition length, but shows a decrease in length as the wake frequency is increased.

Table 2. Constants in the intermittency correlation

Const	Reduced Frequency, Ω			
	1.033	1.725	3.443	5.166
c_1	0.57	0.22	0.50	0.35
c_2	0.80	0.85	0.86	0.88
c_3	1.00	0.82	0.80	0.80
c_4	0.85	0.92	0.92	0.94

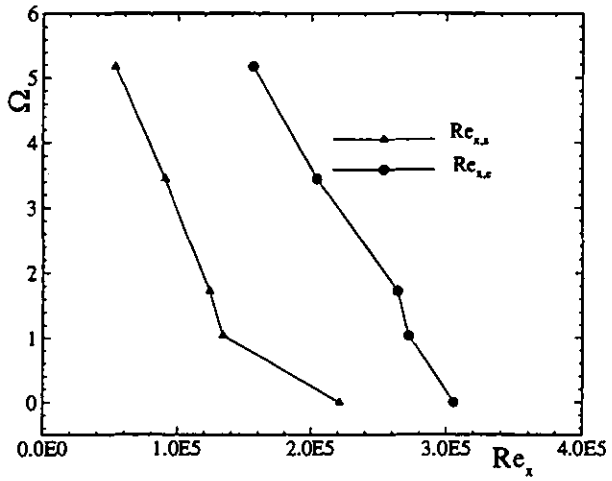

Figure 9. Effect of wake frequency Ω on start and end Reynolds numbers $Re_{x,s}$ and $Re_{x,e}$.

Freestream Turbulence Intensity: One major parameter that affects the boundary layer transition onset is the freestream turbulence intensity. Also, turbulence scales are important as well. They are currently under investigation and their treatment is beyond the scope of this paper. The presence of wakes, particularly their spacing and interaction, contributes significantly to an increase of the freestream turbulence. Figure 10 shows the freestream time-averaged turbulence intensity distribution as a function of inlet wake frequency. For the investigated reduced frequency range, it is observed to approach a maximum value of 4.2% as the wake frequency is increased.

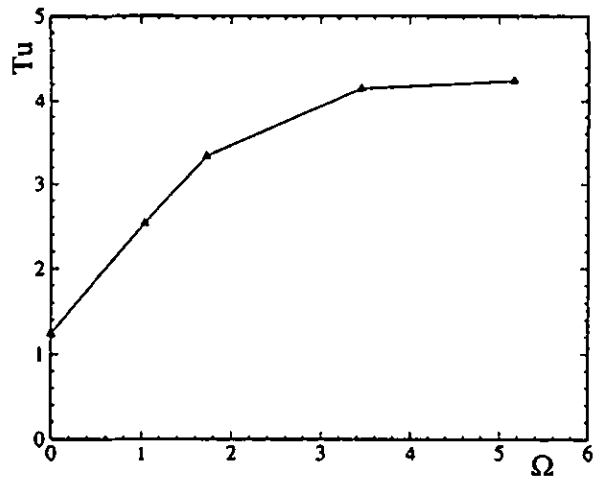

Figure 10. Time-averaged inlet freestream turbulence intensity as a function of Ω.

4. Implementation of the Transition Model into Calculation Procedures

The developed transition model can be implemented into any Navier-Stokes or differential boundary layer code. We have chosen TEXSTAN, which simultaneously solves differential equations of continuity, momentum, and energy. All these equations are time-averaged and are written to describe the flow over an axisymmetric body. The time averaged momentum equation in the x-direction is:

$$\rho U\frac{\partial U}{\partial x} + \rho V\frac{\partial U}{\partial y} = -\frac{dp}{dx} + \frac{1}{r}\frac{\partial}{\partial y}\left[r\left(\mu\frac{\partial U}{\partial y} - \rho\,\overline{u'v'}\right)\right] \tag{10}$$

In this momentum equation, the turbulent shear stress is modeled by the eddy diffusivity for momentum and is defined as

$$-\overline{u'v'} = \epsilon_M\frac{\partial U}{\partial y} = \frac{\mu_t}{\rho}\frac{\partial U}{\partial y} \tag{11}$$

where μ_t is the turbulent viscosity which combines with the laminar viscosity to give

$$\mu_{eff} = (\mu + \mu_t) = \rho(\nu + \epsilon_M) \tag{12}$$

Similarly, after introducing the concept of eddy diffusivity for heat, ϵ_H, the energy equation becomes

$$\rho U\frac{\partial I^*}{\partial x} + \rho V\frac{\partial I^*}{\partial y} = \frac{1}{r}\frac{\partial}{\partial y}\left\{ r\left[\frac{\mu_{eff}}{Pr_{eff}}\frac{\partial I^*}{\partial y} + \frac{\mu_{eff}}{J}\left(1-\frac{1}{Pr_{eff}}\right)\frac{\partial}{\partial y}\left(\frac{U^2}{2}\right)\right]\right\} \tag{13}$$

where I^* is the stagnation enthalpy and Pr_{eff} is the effective Prandtl number defined as

$$Pr_{eff} = \frac{\mu_{eff}}{(k/c)_{eff}} = \frac{1 + \frac{\epsilon_M}{\nu}}{\frac{1}{Pr} + \frac{\epsilon_M}{\nu}\frac{1}{Pr_t}} \tag{14}$$

and Pr_t is the turbulent Prandtl number. A constant value of 0.85 is used for Pr_t in the solution process.

The eddy viscosity term is modeled through the mixing length theory and the intermittency model developed in the current investigation is implemented through

$$\epsilon_M = \gamma l^2\left|\frac{\partial U}{\partial y}\right| \tag{15}$$

where l is the mixing length and γ is the intermittency. The expressions developed in Eqns. 7, 8 and 9 are used in the above equation in place of γ. The solution process uses Patankar-Spalding's(1970) omega (non-dimensional stream function) transformation. In stream function coordinates the momentum equation without the body forces becomes

$$U\frac{\partial U}{\partial x} + U\frac{\partial}{\partial \psi}\left[U\nu_{eff}\frac{\partial U}{\partial \psi}\right] = -\frac{1}{\rho}\frac{dp}{dx} \tag{16}$$

The boundary layer equations are integrated after non-dimensionalizing the stream function and solved numerically through mixing length model. Here, Eqn. 12 and Eqn. 15 are used for solving momentum equation, Eqn. 16. Similarly, Eqn. 14 and Eqn. 15 are used for solving the energy equation, Eqn. 13.

5. Results and Discussions, Aerodynamic Study

5.1 Experimental Results, Intermittency Distribution

The entire set of ensemble-averaged data was utilized to generate the temporal-spatial distribution of the ensemble-averaged turbulence intermittency. Figures 5a and 5b show a few cases as representative examples at y = 0.1 mm. As shown in Fig. 5 (a) (Ω = 1.033, 3 rods), the boundary layer is periodically disturbed by the wakes that cause periodically high turbulence strips and *extended becalmed regions*. These extended becalmed regions were produced by strong damping of turbulence fluctuations in the wall region that leads to an exponential decrease of the maximum intermittency $<\gamma_i(t_i)>_{max}$. These regions are observed between the leading edge and the streamwise position of $s/s_o > 0.4$. As seen, the wake strips are separated from the becalmed regions indicating the absence of any visible interaction near the leading edge. Increasing the frequency Ω of the wake by reducing the rod spacing (Fig. 5b with Ω = 3.443, 10 rods) results in an earlier transition start compared to the above 3 rod case. Two mechanisms are considered instrumental in affecting the above transition start. The first one is an earlier mixing of the wakes due to the reduction of their spacing that leads to higher freestream turbulence, which inherently affects the onset of the transition. The second mechanism is the increased impinging frequency of the primary wake strips that introduce an excessive turbulent kinetic energy transport to the boundary layer causing a shift of transition start toward the leading edge. It is conceivable that the combination of these two mechanisms would make additional contribution to the shift of the transition start. Further increase of Ω results in a higher freestream turbulence and increased impinging frequency and thus a significant shift of the transition toward the leading edge as the consequence of the mechanisms discussed above. A similar turbulence intermittency pattern is observed for other y - positions.

5.2 Calculation Results, Velocity Distributions

The implementation of the intermittency model into the calculation procedure enables the prediction of time-averaged velocity distribution. As representative examples, the time averaged velocity profiles for Ω = 0 and 1.725 are plotted in Figs. 11(a,b) for the laminar, transitional, and turbulent flow regions. These are obtained by using the expression for time-averaged intermittency developed in Eqn. 9 in the solution process. The solid lines exhibit the calculation results, which are in good agreement with the experimental results represented by symbols. It can be seen from Fig. 11b that the transition starts much earlier for Ω = 1.725(5-rods) when compared to Ω = 0.0(No-rods) case shown in Fig. 11a.

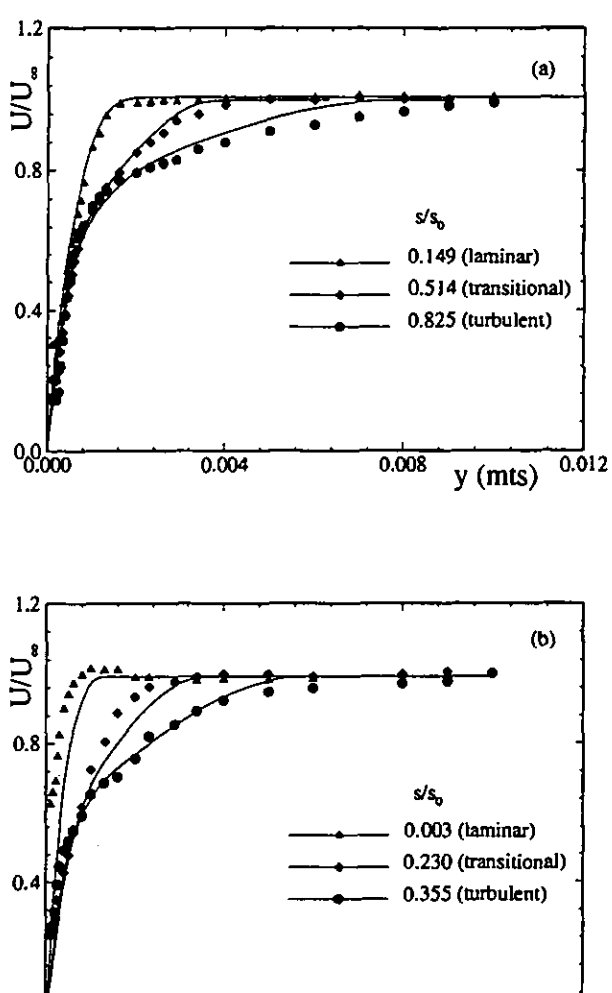

Figure 11(a and b). Velocity profiles as a function of lateral coordinate for three axial locations for (a) Ω = 0.0(No-rods) and (b) Ω = 1.725(5-rods).

6. Results and Discussions, Heat Transfer Study

6.1 Heat Transfer Coefficient Calculation

The heat transfer coefficient is calculated from the following expression

$$h = \frac{Q_{foil} - Q_{rad}}{(T_{yl} - T_\infty)} \qquad (17)$$

where Q_{rad} is the radiation heat loss from the surface of the curved plate, Q_{foil} is the heat flux of the inconel foil, T_{yl} is the yellow line temperature and T_∞ is the free-stream temperature. Q_{foil} and Q_{rad} are given by:

$$Q_{foil} = \frac{VI}{A_{foil}} \qquad (18)$$

and

$$Q_{rad} = \epsilon\sigma(T_{yl}^4 - T_\infty^4) \qquad (19)$$

where V and I are the voltage and current supplied from the power supply respectively, and A_{foil} is equal to the total heat transfer surface area of the Inconel 600 foil. Finally, the Stanton number is defined by:

$$St = \frac{h}{\rho C_p \overline{U}} \qquad (20)$$

6.2 Heat Transfer, Steady Inlet Flow Reference Case

As indicated previously, we used liquid crystal technique for heat transfer measurement, which is developed by Hippensteele (1981), and is being applied by numerous researchers. It has the advantage of not affecting the turbulence structure at the surface, as thermocouples or surface mounted hot wire/film probes do. However, its slow response does not allow extracting valuable unsteady information. As a result, in unsteady cases, only time-averaged response can be acquired. Using this technique, first for comparison purposes, the steady state case $\Omega = 0$ (no-rod) is presented in Fig. 12, where the above model is applied. Good agreement between calculation and experiment is shown in Fig. 12 for a wide range of Re_x from leading edge via transition portion to trailing edge. For comparison purposes, Mayle's model(1991) shows some discrepancies between the experiment and theory. However, it should be pointed out that Mayle's correlation gives reasonably good results for time-averaged unsteady cases.

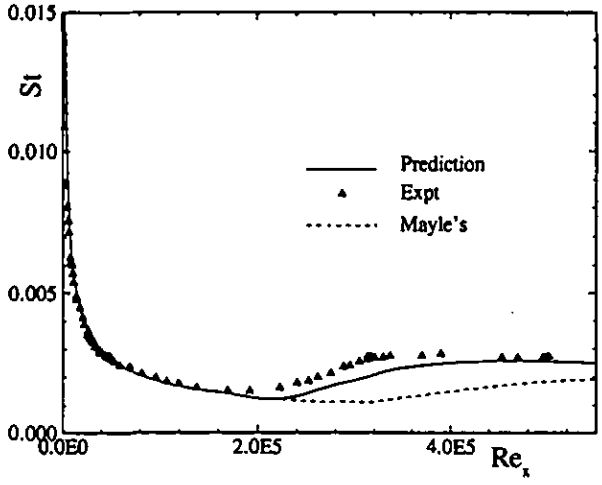

Figure 12. Heat transfer coefficients as a function of axial Reynolds number for no-rod or steady case.

6.3 Heat Transfer, Unsteady Inlet Flow Cases

For unsteady flow cases with a reduced frequency(see Table 1) values of $\Omega = 1.033$ and 5.166, calculated Stanton numbers are compared with the experimental results and shown in Figs. 13a and b, where the experimental results are represented by symbols. Furthermore, three curves are plotted in each diagram representing the calculation results. Starting with a reduced frequency of $\Omega = 1.033$ (3 rods), the upper solid curve represents the streamwise Stanton number distribution when the plate is subjected to an inlet flow intermittency state of $\langle\gamma(t)\rangle_{max}$. On the other hand, if the plate

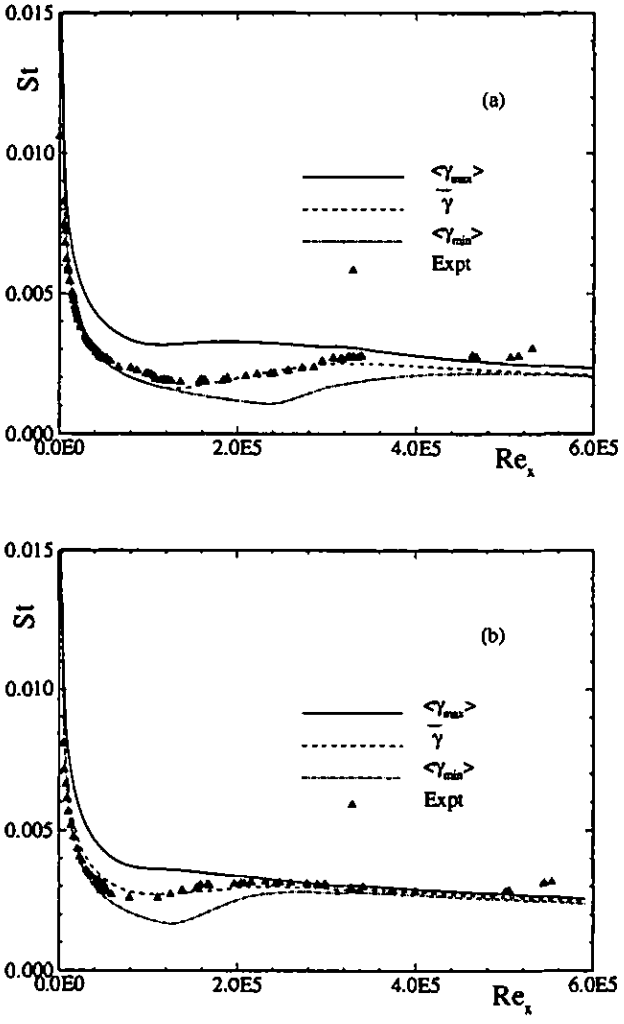

Figure 13(a and b). Heat transfer coefficients as a function of axial Reynolds number for (a) $\Omega = 1.033$(3-rods) and (b) $\Omega = 5.166$(15-rods).

is subjected to $<\gamma(t)>_{min}$, the lower point-dashed curve depicts its Stanton number distribution. However, because of the periodic character of the inlet flow associated with unsteady wakes, the plate would experience a periodic change of heat transfer represented by upper and lower Stanton number curves (solid line and point-dashed line) as an envelope. The liquid crystal responds to this periodic event with time averaged signals. This time-averaged result is reflected by the dashed line, which gives a corresponding time averaged intermittency. As seen, a reasonably good agreement is found for the entire laminar and transitional portions. Close to the plate trailing edge, the theory under predicts slightly. It should be mentioned that in this area, heat transfer measurements were associated with certain difficulty.

As the experimental results (symbols in Fig. 13b) show, increasing the reduced frequency to $\Omega = 5.166$ (15 rods), causes the transition point to shift toward the leading edge, resulting in a slightly higher Stanton number. This shift of the transition point is in full accord with the aerodynamic findings explained previously. Similar to the case with $\Omega = 1.033$, the upper solid curve represents the streamwise Stanton number distribution if the plate is subjected to an inlet flow intermittency state of $<\gamma(t)>_{max}$. The lower point-dashed curve depicts the Stanton number distribution pertaining to the minimum intermittency $<\gamma(t)>_{min}$. The time averaged result is reflected by the dashed curve, which gives a corresponding time averaged intermittency. Figure 13b exhibits reasonably good agreement between the theory and experiment in the transition and turbulent regions with $Re_x > 1.2x10^5$. In the laminar region, however, the theory slightly over predicts the heat transfer resulting in marginally higher Stanton numbers. In this region, better agreement can be reached by utilizing the minimum intermittency $<\gamma(t)>_{min}$. Similar tendencies are seen for other Ω's of 1.725(5 rods) and 3.443 (10 rods). As discussed previously, a combined effect of wake mixing and the increased impinging frequency of the wake strips that introduce an excessive turbulent kinetic energy transport to the boundary layer cause a shift of transition start toward the leading edge.

7. CONCLUSIONS

A transition model that includes the effects of periodic unsteady wakes on the boundary layer and heat transfer of a concave surface of a curved plate is developed for zero pressure gradient. Instantaneous velocities using hot wire anemometry are measured in the boundary layer for four wake passing frequencies. Steady or no-wake case is also used to determine the intermittency distribution inside the boundary layer. The method of Hedley and Keffer is used to distinguish between turbulent and laminar parts in the instantaneous velocity signals and the result is ensemble averaged to give ensemble averaged intermittency. Based on the results from these investigations, the following conclusions are drawn.

1.) The unsteady wake flow periodically changes the boundary layer transition from natural transition to wake induced transition depending on the presence of turbulent core inside the wake region.

2.) A transition model has been developed that includes the effects of periodic unsteady flow on the boundary layer transition on a curved plate.

3.) The relative intermittency factor is seen to follow a gaussian distribution. The minimum intermittency factor, $<\gamma_{min}>$, represents the boundary layer behavior in between the turbulent wake strips. It is shown to follow the natural transition process as the free-stream is almost non-turbulent. On the other hand, $<\gamma_{max}>$ being the value inside the turbulent core, starts with a value of 1.0 and goes through a minimum. This is due to the viscous damping of the turbulent core by the boundary layer.

4.) The transition process starts earlier as the wake frequency is increased. The length of wake-induced transition is higher when compared to the steady case. However, wake-induced transition length decreases as the wake frequency is increased.

5.) The heat transfer coefficients and the velocity distribution by the numerical solution using the developed transition model compare well with the experimental data and the maximum and the minimum limits of heat transfer coefficients are predicted.

ACKNOWLEDGEMENTS

The authors would like to express thanks and appreciation to Mr. Hippensteele of NASA Lewis Research Center for his advice on liquid crystal instrumentation and to Prof. M. Crawford for making TEXSTAN available to them. They also would like to thank DOE for support of this research.

REFERENCES

Abu-Ghannam, B. J., and Shaw, R., 1980, "Natural Transition of Boundary Layers-The Effects of Turbulence, Pressure Gradient and Flow History," *J. Mech. Eng. Sci.*, Vol. 22, pp. 213-228.

Antonia, R. A., and Bradshaw, P., 1971, *Imp. College Aero. Rep.* No. 71-04.

Bradshaw, P., and Murlis, J., 1973, *Imp. College Aero. Tech. Note*, No. 73-108.

Crawford, M. E., and Kays, W. M., 1976, "STAN5 (TEXSTAN version)-A Program for Numerical Computation of Two Dimensional Internal and External Boundary Layer

Flow," NASA CR-2742.

Dhawan, S., and Narasimha, R., 1958, "Some Properties of Boundary Layer Flow During The Transition From Laminar to Turbulent Motion," *Journal of Fluid Mechanics*, Vol. 3, pp. 418-436.

Dullenkopf, K., Mayle, R. E., 1994, ASME Paper No. 94-GT-174.

Eifler, J., 1975, "Zur Frage der freien turbulenten Strömungen, insbesondere hinter ruhenden und bewegten Zylindern," Dissertation D-17, Technische Hochschule Darmstadt, Germany.

Emmons, H. W., 1951, "The Laminar-Turbulent Transition in Boundary Layer-Part I," J. Aero. Sci., Vol. 18, pp. 490-498.

Gostelow, J. P., and Blunden, A. R., 1989, "Investigations of Boundary Layer Transition in an Adverse Pressure Gradient," ASME *Journal of Turbomachinery*, Vol. 111, pp. 366-375.

Gostelow, J.P., Melwani, N., and Walker, G.J., 1995, "Effects of Streamwise Pressure Gradient on Turbulent Spot Development," ASME Paper No. 95-GT-303.

Gostelow, J. P., and Ramachandran, R. M., 1983, "Some Effects of Free Stream Turbulence on Boundary Layer Transition," *Proceedings of 8th Australasian Fluid Mechanics Conference*.

Halstead, E. D. et al., 1995, "Boundary Layer Development in Axial Compressors and Turbines: Parts 1 to 4," ASME Paper No. 95-GT-461 to 464.

Hedley, B. T., and Keffer F. J., 1974, "Turbulent/Non-Turbulent Decisions in an Intermittent Flow," *Journal of Fluid Mechanics*, Vol. 64, pp. 625-644.

Herbst, R., 1980, "Entwicklung von Strömung-grenzsschichten bei instationärer Zuströmung in Turbomaschinen," Dissertation D-17, Technische Hochschule Darmstadt, Germany.

Hippensteele, S. A., Russell, L. M., and Stepka, S., 1981, "Evaluation of A Method for Heat Transfer Measurements and Thermal Visualization Using a Composite of a Heater Element and Liquid Crystals," ASME *Journal of Heat Transfer*, Vol. 105, pp. 184-189.

Hodson, H.P., 1990, "Modeling Unsteady Transition and Its Effects on Profile Loss," *Journal of Turbomachinery*, Vol. 112, pp. 691-701.

Kovasznay, L.S.G., Kibens, V. and Blackwelder, R.F., 1970, *J. Fluid Mech.*, Vol. 41, pp. 283.

Launder, B. E., and Spalding, D.B., 1972; *Mathematical Models of Turbulence*, Academic Press, New York.

Liu, X., and Rodi, W., 1992, "Measurement of Unsteady Flow and Heat Transfer in a Linear Turbine Cascade," ASME Paper No. 92-GT-323.

Mayle, R. E., 1991, "The Role of Laminar-Turbulent Transition in Gas Turbine Engines," *Journal of Turbomachinery*, Vol. 113, pp. 509-537.

Narasimha, R., 1957, "On the Distribution of Intermittency in the Transition Region of a Boundary Layer," *J. Aero. Sci.*, Vol. 24, pp. 711-712.

Orth, U., 1992, "Unsteady Boundary-Layer Transition in Flow Periodically Disturbed by Wakes," ASME Paper No. 92-GT-283.

Pache, W., 1976, "Zur Frage der Entwicklung von Strömungsgrenzsschichten bei instationärer Zuströmung in Turbomachinen," Dissertation D-17, Technische Hochschule Darmstadt Germany.

Patankar, S. V., and Spalding, D. B., *Heat and Mass Transfer in Boundary Layers*, 2nd Ed., International Textbook Company Ltd., London, 1970.

Paxson, D.E., Mayle, R.E., 1991, "Laminar Boundary Layer Interaction With an Unsteady Passing Wake," *Journal of Turbomachinery*, Vol. 113, pp. 419-427.

Pfeil, H., and Herbst, R., 1979, "Transition Procedure of Instationary Boundary Layers," ASME Paper No. 79-GT-128.

Pfeil, H., Herbst, R., and Schröder, T., 1983, "Investigation of the Laminar-Turbulent Transition of Boundary Layers Disturbed by Wakes," ASME *Journal of Engineering for Power*, Vol. 105, pp. 130-137.

Schmidt, R.C., and Patankar, S.V., 1991, "Simulating Boundary Layer Transition With Low-Reynolds-Number k-ϵ Turbulence Models: Part I-An Evaluation of Prediction Characteristics; Part II-An Approach to Improving the Predictions," *Journal of Turbomachinery*, Vol. 113, pp. 10-26.

Schobeiri, M. T., 1979, "Theoretische und experimentelle Untersuchungen laminarer und turbulenter Strömungen in Diffsoren," Dissertation D-17, Technische Hochschule Darmstadt, Germany.

Schobeiri, M. T., and Radke, R., 1993, "Effects of Periodic Unsteady Wake Flow and Pressure Gradient on Boundary Layer Transition Along The Concave Surface of A Curved Plate," ASME Paper No. 94-GT-327.

Schobeiri, M. T., Read, K., and Lewalle, J., 1995, "Effect of Unsteady Wake Passing Frequency on Boundary Layer Transition: Experimental Investigation and Wavelet Analysis," ASME Paper No. 95-GT-437.

Walker, G.J., 1989, "Modeling of Transitional Flow in Laminar Separation Bubbles," *9th Int. Symp. Air Breathing Engines*, pp. 539-548.

Wright, L., Schobeiri, M. T., 1996, "Effect of Unsteady Wake Flow on Heat Transfer Along a Concave Surface," to be submitted.